24th Australasian Fluid Mechanics Conference – AFMC2024
Canberra Australia
1-5 December 2024

Paper No: AFMC2024-028
DOI:10.5281/zenodo.14213417

Hybrid Velocity Measurements: A Comparison of the roving Preston tube and Prandtl-Pitot tube

Jason Harley [1*] and Hubert Chanson [1]

[1] School of Civil Engineering, The University of Queensland, Brisbane QLD 4072, Australia
* Email: j.harley@uq.net.au

Abstract

The measurement of velocity in confined open channel geometries presents challenges that require the application of hybrid physical modelling techniques. Herein, velocity measurements were performed using the Prandtl-Pitot tube and the roving Preston tube (RPT). Each instrument has unique limitations in terms of measurement accuracy and ability to reach particular locations within a flow cross-section. When these instruments were collectively applied as a measurement suite, they overcome these limitations whilst providing useful measurement verification. The focus of this paper is the RPT, whose operations relied on reference pressure readings that varied with distance from flow boundaries. To address these variations, the RPT previously relied on bulk calibration methods to adjust measured velocities. But these methods resulted in inaccurate representations of time-averaged velocity, especially near boundaries. To investigate this limitation, the roving Preston tube was tested in a wind tunnel to investigate wall effects on reference pressures. To complement this physical investigation, large eddy simulation (LES) numerical modelling was conducted to evaluate kinematic structures located at the orifice of the reference pressure tube and provide insight into why pressures vary with distance from fixed boundaries.

1. Introduction

In terms of measurement characteristics, the Prandtl-Pitot tube can consistently measure reference pressures (static pressures), despite an inability to access some confined geometries. The roving Preston tube (RPT) is a small compact tube assembly used to measure flows close to boundaries and within complex geometries Macintosh & Isaacs (1992). The RPT's operation relied on reference tube pressure readings that varied with distance from flow boundaries. Numerous studies have previously investigated Prandtl-Pitot tube performance such as Tropea *et al.*, 2007; Chue, 1975; Troskolanski, 1960; and Folsom, 1956, whilst the literature on the RPT was more limited. Consequently, further investigation of the RPT is the focus of this paper.

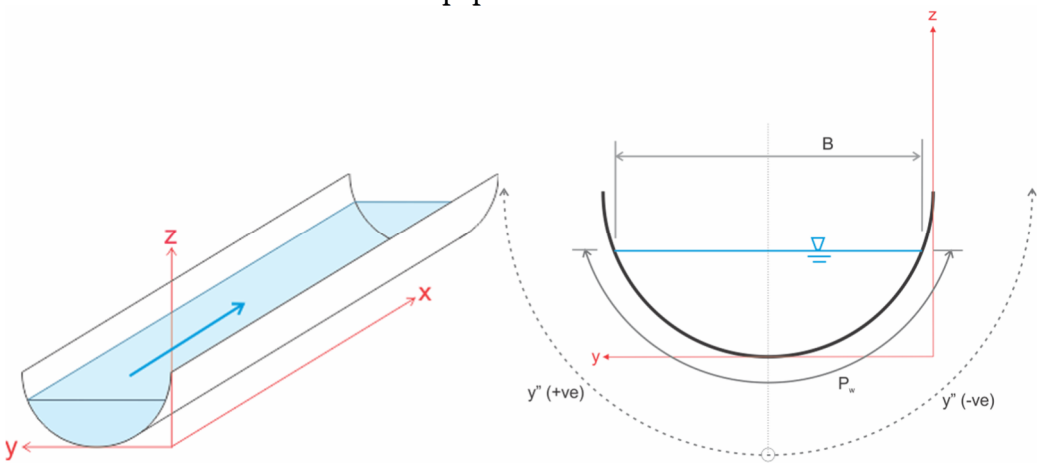

Figure 1. Experimental semi-circular open channel flume. (Left) Coordinate axes for a semi-circular channel where 'x' represents the direction of longitudinal velocity. (Right) semi-circular channel cross section.

2. Experimental Facilities and Instrumentation

2.1 Experimental Facilities

Open channel experiments were conducted at the University of Queensland in a semi-circular PVC channel (D = 0.5m) installed within a 15 m long 0.5 m wide horizontal flume (Fig. 1). Water was supplied by an intake structure, fed by a constant head tank, and equipped with flow straighteners and a three-dimensional converging section leading to the semi-circular section. Downstream, the flume ended with a free overfall. Wind tunnel experiments were conducted in the Unsteady Wind tunnel (UWT) which was a variable speed Eiffel-style wind tunnel comprising of a 760 mm×760 mm test section. Measurements were conducted on a 1200mm long × 600mm flat PVC plate assembly with a sharp front edge and a trip wire set at 5mm above the plate.

2.2 Instrumentation

Time-averaged velocity measurements in the longitudinal direction were measured with a Dwyer™ 166 Series (ϕ = 2.98 mm) Prandtl-Pitot tube (PPT) with a semi hemispherical nose. Velocity was calculated using eq.(1) based on the Bernoulli principle (Troskolanski, 1960).

$$V_x = \sqrt{2\,g\,(h_{1(ppt)} - h_{2(ppt)})\sin\theta_m} \quad (1)$$

where,

$h_{1(ppt)}$ = total head manometer reading of the Prandtl-Pitot tube (ppt) (m)
$h_{2(ppt)}$ = static (reference) pressure head manometer reading of Prandtl-Pitot tube (ppt) (m)
θ_m = angle of the inclined manometer (degrees)

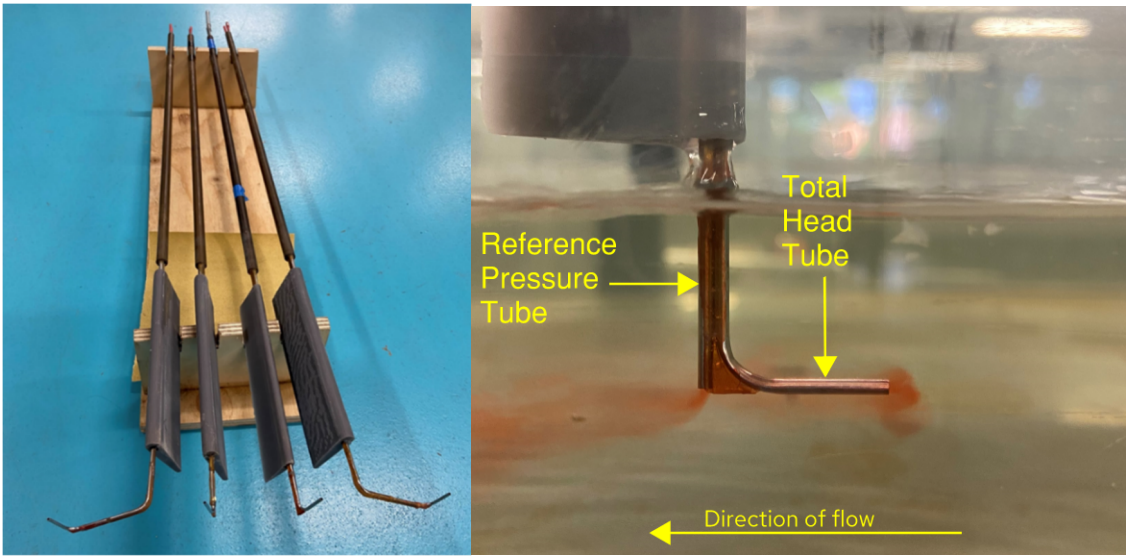

Figure 2. Roving Preston tubes. (Left) RPT variants (left to right): RPT C1.6L; RPT C1.4C; RPT C1.6C; & RPT C1.6R. The RPT C1.6L and RPT C1.6R were fitted with horizontal arms designed to access complex channel geometries. (Right) RPT C1.6C in an open channel water flume whilst being purged with dye.

The expected error was calculated to be 0.01 m/s. Yet, some velocity errors up to 5% were recorded close to the free surface due to possible wake-induced effects on the static pressure holes. Folsom (1955) highlighted this phenomenon, although no reliable a-priori correction method was ever developed. Free surface effects, whilst interesting and relevant to open channel physical experiments, are outside of the scope of this paper.

The RPT comprised of two stainless steel tubes contained within a guide stem (Fig. 2). The outer tube diameters were between 1.42mm to 1.62mm. The total head tube was a 20mm horizontal projection with a sharp-nosed opening. The reference pressure tube was located on the leeward side of the guide stem. Some variants were fitted with horizontal arms to access complex cross-sectional geometries as shown in Figure 2 (Macintosh, 1990; Macintosh & Isaacs, 1992). A symmetrical foil was fitted to reduce vortex shedding and vibrations. For wind tunnel experiments, the Prandtl Pitot tube and RPT were checked against a four-hole Cobra 416 probe fitted with a 2.6mm high probe, to confirm correct operation of both tubes, and was not used for calibration.

2.3 Experimental flow conditions

Open channel experiments were conducted with a horizontal bed slope, resulting in gradually varied subcritical flows. Wind tunnel tests were conducted on a flat plate centrally located within the wind tunnel for varying free stream velocities. Turbulence intensity measured by the Cobra probe ranged from 8-14% for z = 0 m (invert) to 0.2% at z = 0.3m. These values indicated that the trip was operating correctly. A detailed summary of flow measurements is shown in Table 1.

Measurements	Instrumentation	Flow Conditions
Centre-line velocity profiles in a smooth semi-circular open channel (x=7.15m, y=0.25m, D=0.5m)	Prandtl-Pitot tube; RPT (ϕ_{OD} =1.42mm)	Q = 0.025, 0.050, 0.075 m^3/s
Centre-line velocity profiles on a flat plate within a wind tunnel (y=0.30m, W=0.6m)	Prandtl-Pitot tube; RPT (ϕ_{OD} = 1.42mm), Cobra Probe	V= 4.6, 9.8, 14.8 and 21.5 m/s (time-averaged steady state free stream velocity)

Table 1. Instrumentation, Measurements and Flow Conditions.

3. Velocity Measurements

3.1 Open channel centre-line velocity measurements

Open channel measurements for the Prandtl Pitot tube and the RPT were shown in Figure 3. The magnitude of RPT velocities derived from eq. (1) were typically higher than the Prandtl Pitot tube. This increase appeared to be primarily caused by the measurement of a static pressure deficit by the RPT reference pressure tube, resulting in all RPT measurements requiring some degree of calibration.

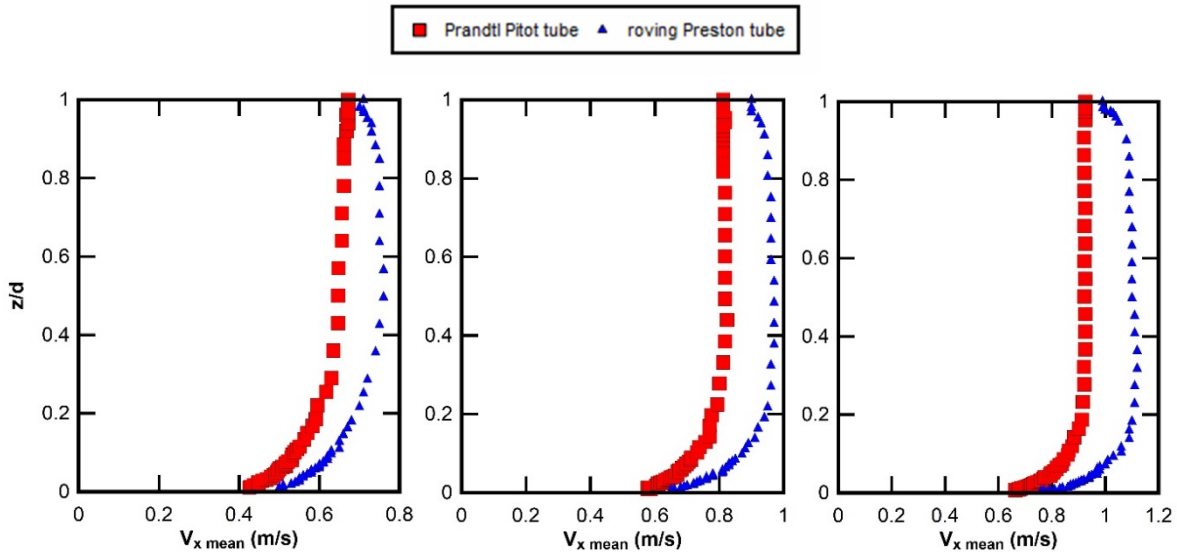

Figure 3. Comparative centre-line longitudinal time-averaged local velocity ($V_{x\ mean}$) of water in a smooth semi-circular channel, y=0.25m, D=0.5m. (Left) Q=0.025m^3/s, (Middle) Q=0.050 m^3/s, (Right) Q =0.075 m^3/s. Note: RPT velocities were derived from eq. (1) and were thus uncalibrated.

The magnitude of RPT velocities for z/d > 0.8 slightly reduced as it approached the free surface due to higher RPT reference pressure tube readings. In comparison, Prandtl Pitot tube velocities for z/d > 0.8 remained constant, and this could be attributed to its design which had 8 small pressure tappings, equally spaced around the tube circumference, and located at least 2 x ϕ_{OD} from the nose. It was hypothesized that this tube arrangement ensured that any localised differences in static pressure around the tube circumference could be 'averaged' out. These effects were not observed in RPT wind tunnel experiments due to the absence of a free surface, as air was the only phase present.

3.2 Wind tunnel flat plate centre-line velocity measurements

Wind tunnel flat plate centre-line velocity measurements were shown in Figure 4. Similar to the open channel experiments, RPT reference tube pressures were lower than the Prandtl Pitot tube static pressures. This difference caused an overestimation of velocity magnitude when the Bernoulli relationship (eq. 1) was applied. Figure 4 also showed that the shape of the RPT velocity gradient agreed well with the Prandtl Pitot tube.

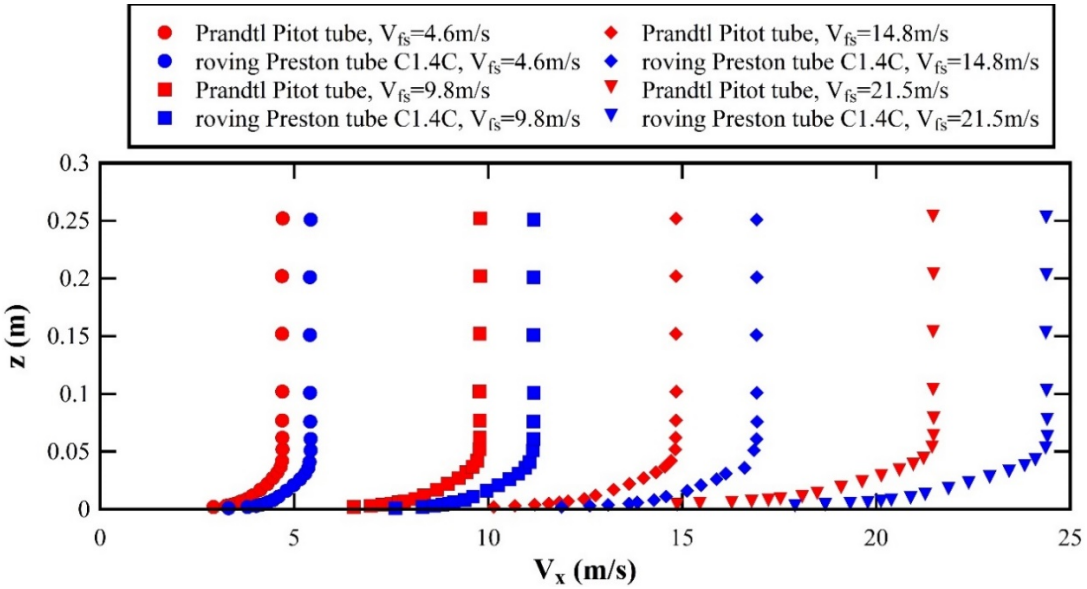

Figure 4. Comparative centre-line longitudinal time-averaged local velocity ($V_{x\ mean}$) of air on a flat plate in a wind tunnel, y=0.3m, W=0.6m. The average freestream velocity, V_{fs}, was stated in the legend. Similar to Fig 3, RPT velocities were derived from eq. (1) and were thus uncalibrated.

3.3 Calibration of the RPT

Early RPT studies employed the Patel calibration method for channel measurements (Macintosh, 1990). However, recent studies have applied depth-averaged calibrations against Prandtl-Pitot tube readings based on the following equation (Sanchez *et al.*, 2018 & 2021; Chanson, 2020):

$$V_x = \frac{1}{\lambda}\sqrt{2\ g\left(h_{1(rpt)} - h_{2(rpt)}\right)\sin\theta_m} \qquad (2)$$

where,

λ = the RPT bulk velocity correction factor.

$h_{1(rpt)}$ = total head manometer reading of the RPT (rpt) (m)

$h_{2(rpt)}$ = reference pressure head manometer reading of the RPT (rpt) (m)

The coefficient, λ, was the ratio of Prandtl-Pitot tube derived depth-averaged velocity with the RPT derived depth-averaged velocity velocities, $\frac{1}{d}\left(\int_0^d V_{x(ppt)}\ dz\right) = \frac{1}{\lambda}\frac{1}{d}\left(\int_0^d V_{x(rpt)}\ dz\right)$.

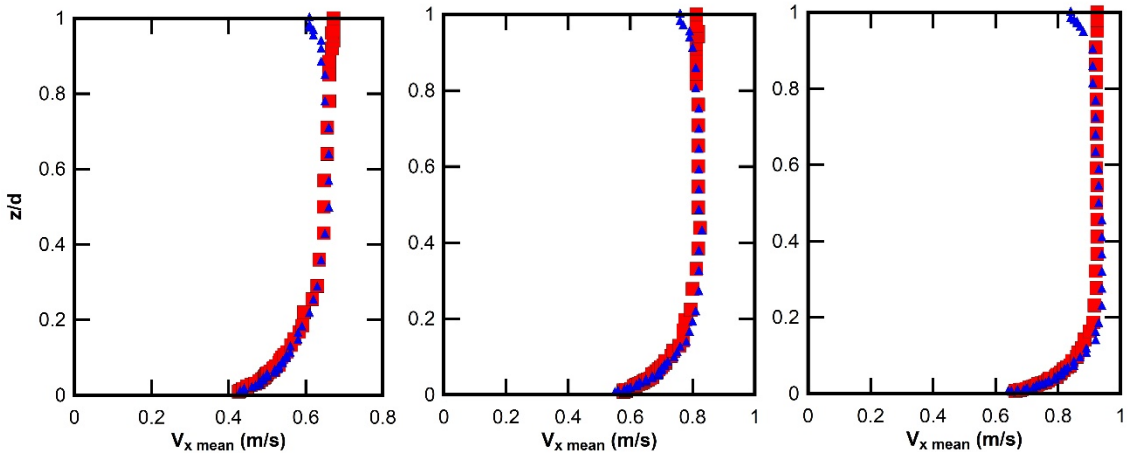

Figure 5. Depth-averaged calibration of RPT velocity using eq. (2) compared to the Prandtl Pitot tube derived velocity for measurements in water (Left)Q=0.025m^3/s,(Middle)Q=0.050 m^3/s,(Right)Q =0.075 m^3/s.

The calibrated velocities for water experiments were shown in Figure 5. For this study, the RPT velocity calibration factor λ varied between 1.15 to 1.19, similar to the value λ = 1.2 obtained by Sanchez *et al.* (2018). However, calibrated velocities were overestimated near the invert, with implications for boundary shear stress calculations. An inspection of readings showed that the total head tube readings were generally identical between the Prandtl-Pitot tube and RPT, in both air and water. However, RPT reference pressure tube readings differed from Prandtl-Pitot tube static pressure

readings depending on the distance from fixed boundaries and flow conditions. A dimensional analysis showed that the relevant parameters influencing the operations of the RPT included:

$$\Pi\left(V_{mean}, D_H, \rho, \mu, \phi_{OD}, \frac{dV_x}{dz}, z, d \right) \quad (3)$$

This analysis resulted in the development of a relationship to quantify the pressure deficit between the RPT reference tube pressure and the Prandtl Pitot tube static pressure for identical flow and proximity conditions. This pressure deficit was found to be minimal at fixed boundaries, and then increased monotonically, eventually approaching an asymptote when tube readings reached a distance of 30-40 x ϕ_{OD} away from fixed boundaries. Further quantification of this pressure deficit was adapted from the pressure coefficient relationship (Birkhoff & Zarantonello, 1957).

$$C_p = \frac{p_o - p_r}{\frac{1}{2}\rho V_x^2} \quad (4)$$

where,

C_p = pressure coefficient
p_r = measured reference tube pressure (Pa)
p_o = measured static pressure (Pa), based on Prandtl-Pitot tube readings
V_x = local time-averaged velocity based on Prandtl-Pitot tube readings (m/s)
Re_t = Reynolds tube number, based on local time-averaged velocity and outer tube diameter.

Eq. (4) was applied to air and water experimental data and plotted against the Reynolds tube number (Fig. 6). C_p did not conveniently collapse into a single curve and was flow dependent. Attempts to curve-fit the C_p - Re_t relationship, along with trialing other dimensionless combinations, proved unsuccessful.

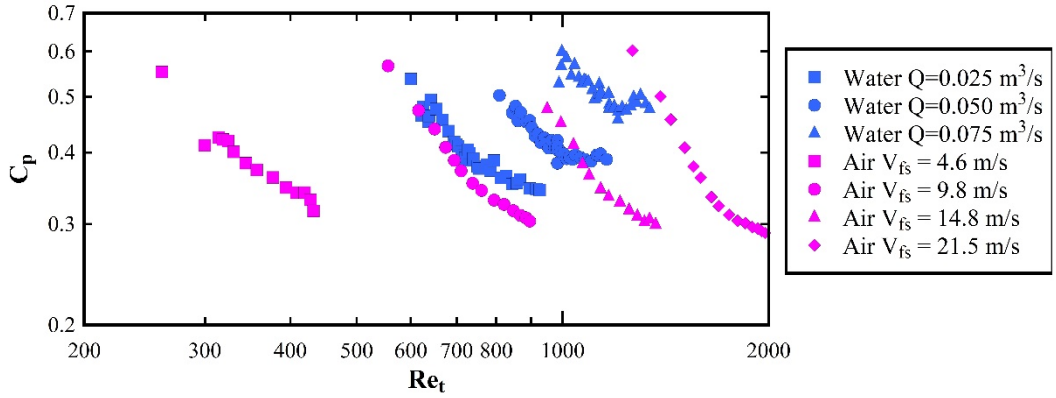

Figure 6. Relationship between RPT pressure coefficient (C_p) and local Reynolds tube number (Re_t) for air and water experiments (Log/ Log plot).

4. LES numerical simulation of the roving Preston tube

A Large Eddy Simulation (LES) was conducted to evaluate the kinematic flow structures located near the reference tube orifice and provide further insight into the existence of static pressure deficits.

Software Settings	Details
General	3d, double precision, pressure based, transient
Bounding Box	121.4mm (L) x 65.1mm (H) x 41.4mm (W)
Mesh	7,409,565 cells (Poly-hexcore)
Mesh Size	Minimum 0.1mm, Maximum 1.6mm
LES Subgrid Scale model	Kinetic Energy Transport
Time / Discretization	Bounded 2nd Order Implicit (Time) 2nd Order / SIMPLEC (Pressure) Bounded Central Differencing (Momentum and Subgrid Kinetic Energy)
Turbulence	TI=5%, Turbulent Viscosity Ratio = 10, with Vortex Method

Table 2. Numerical Simulation Details (water).

The simulation was implemented in ANSYS Fluent 2023 R1. The total head tube orifice face was set at x = 0 m. The measured centreline velocities from Q=0.075 m^3/s water experiments were used as input for the velocity-inlet boundary condition. Several observations were made. Firstly,

streamlines originating from sources upstream of the total head tube orifice did not match streamlines observed near the reference tube orifice as shown in Figure 7. This observation did not accord with the assumption that both total head tube pressures and reference tube pressures belong to the same streamline and cast doubt on the validity of applying Bernoulli's relationship to RPT operations.

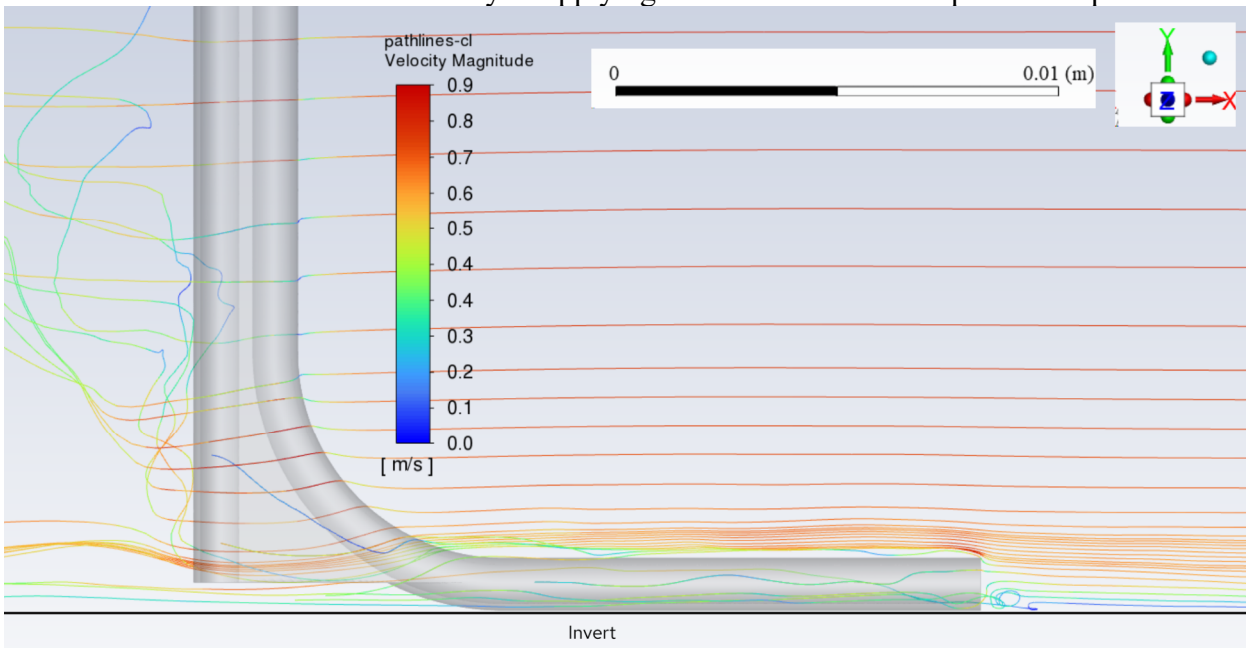

Figure 7. Streamline plot for the LES simulation of RPT C1.4C, plot in the x-y plane at z = 0 m, RPT position is y = 0 m (total head tube lying on the invert), Q=0.075m^3/s case)

Total pressure and static pressure along the centreline axis of the total head tube was also examined. Figure 8 showed that total pressure abruptly changed near the reference tube orifice (x = -0.02069 m). This was possibly caused by flow immediately encountering the deep cavity of the reference tube. The identification of this pressure deficit within the reference tube orifice zone was an important finding, which aligned with the experimental data and further confirmed the difficulty of applying the Bernoulli relationship to RPT operations.

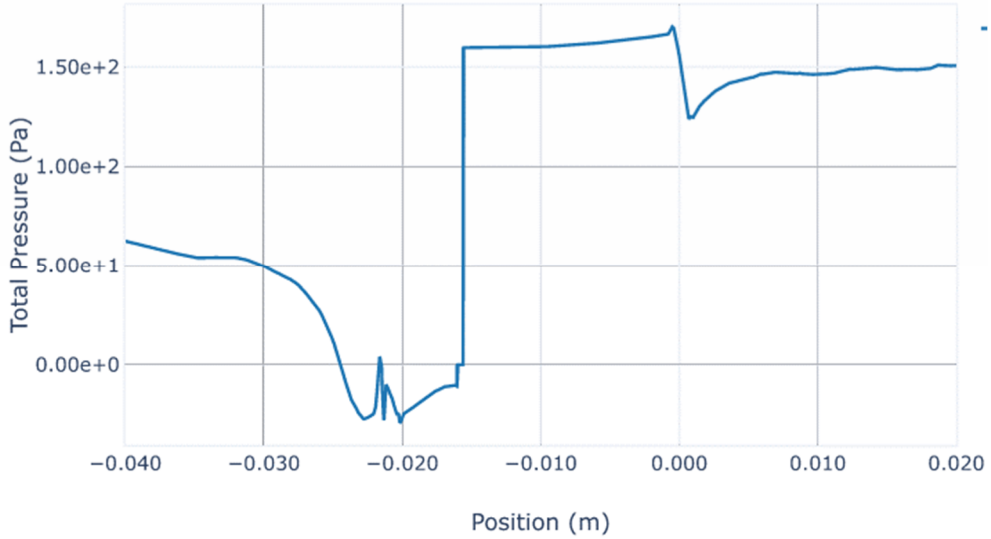

Figure 8. Total pressure (Pa) along the total head tube centreline (x-direction) for the LES simulation of RPT C1.4C, z = 0 m, y = 0.00071 m, RPT position y = 0 m (lying on invert).

Of note in Figure 8 was the slight increase of total pressure inside the total head tube (between x =-0.002 m to -0.015m), compared to total pressure measured along the equivalent approaching flow axis (between x = 0.020 m and 0.005m).This slight pressure increase was attributed to the influence of local velocity gradients, due to the presence of the total head tube which tended to 'deflect' streamlines towards the region of lower velocity, causing the total head tube to measure pressure more than what would normally be measured at the same location in the absence of the total head

tube. This velocity displacement effect has been well documented by researchers such as Chue, 1975 and Bailey *et al*. 2014. Also noted was the abrupt pressure change within the immediate stagnation zone of the total head tube orifice (between x = -0.002 to 0.003 m). The pressure deficit measured at x =0.001 m appeared to have substantially recovered within a distance of $1\times\phi_{OD}$ from the front orifice face, with complete total pressure recovery observed within 10mm of the front orifice face at x = -0.010 m (inside the total head tube).

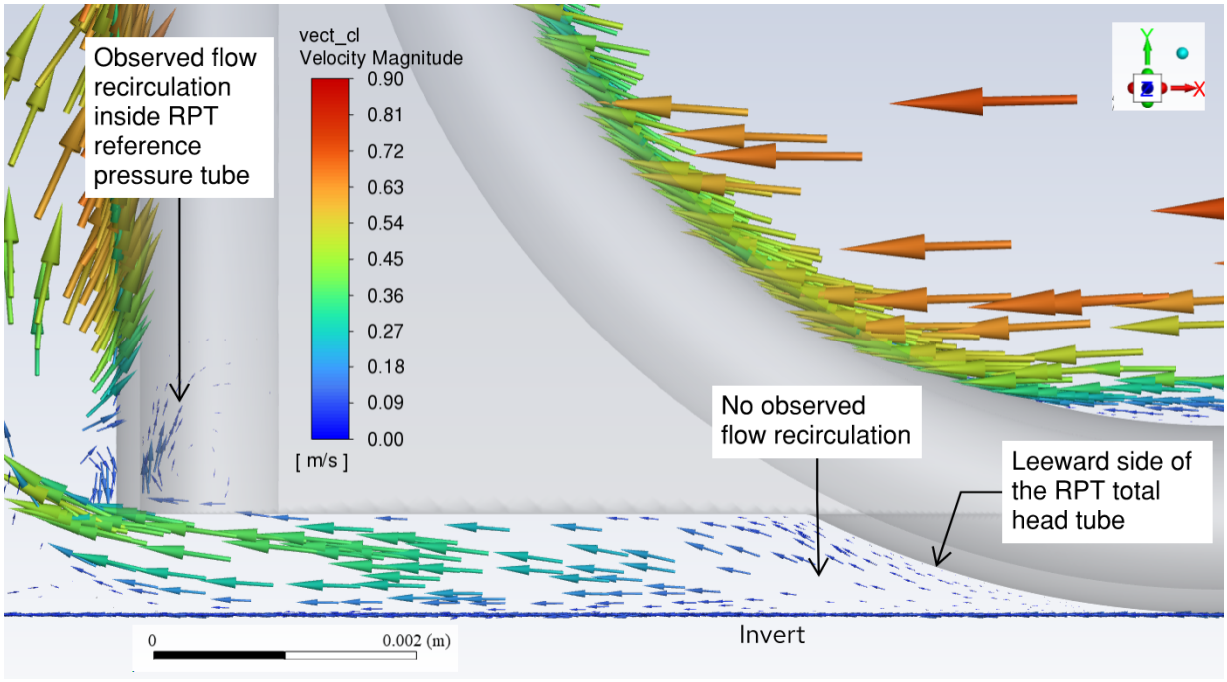

Figure 9. Velocity vector plot for the LES simulation RPT C1.4C, closeup near the reference tube orifice, plot in the x-y plane at z = 0 m, RPT position y = 0 mm (lying on invert), Q = 0.075 m^3/s

Velocity vector plots in the flow region between the invert, leeward side of the total head tube (x = -0.016 m) and the reference pressure tube orifice (x = -0.02069 m) showed no flow recirculation (Fig. 9). Once past the total head tube (x = - 0.013 m), flow did not appear to separate from the curved rear of the total head tube. The leeward side of this curved tube did not appear to behave like canonical 'backstep' flow, but more akin to attached flow moving past the top chord of the aerofoil. A small coherent recirculation zone was also observed inside the reference pressure tube with velocities less than 0.1 m/s. Longitudinal velocities, between the main body of the RPT tube and the invert began to recover and were approximately 0.25-0.30 m/s. This localised velocity recovery may be partly responsible for the pressure deficit recorded in the region surrounding the reference tube orifice.

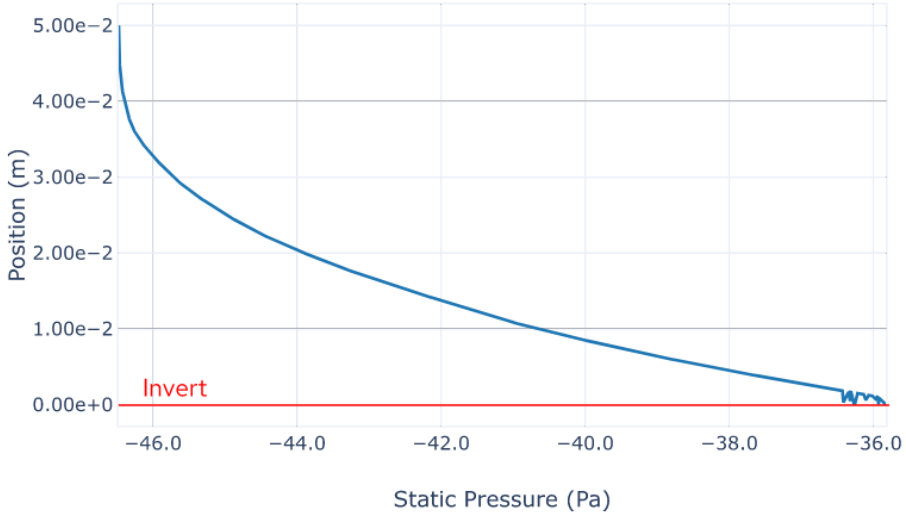

Figure 10. Static Pressure (Pa) along the reference pressure tube centreline for the LES simulation of RPT C1.4C, plot at x= -0.02069 m, between y= 0.000m (invert) to y=0.05m, z= 0 m.

Finally, the measurement of static pressure along the centreline of the reference pressure tube (Fig. 10), showed that the static pressure deficit did not approach a constant value until approximately 50mm up inside the reference pressure tube (30-35 x ϕ_{OD}). The hydrodynamics observed inside the reference pressure tube was akin to skimming flow past a deep cavity. However, velocity magnitude inside the reference pressure tube was small (<0.1 m/s) and was unable to provide insight into why the magnitude of static pressure was still decreasing well within the reference pressure tube cavity.

Whilst only a single numerical simulation was conducted, a comparison with experiment results is shown in Table 3. The difference between results appeared reasonable (15%) considering the limits of experiment error and the power curve fit approximation of experimental velocity inputted into Ansys Fluent as a velocity inlet boundary condition.

Numerical Simulation			Experimental Results		Difference between Numerical and Experimental Results
Total Pressure (Pa)	Reference Pressure (Pa)	Δ P (Pa)	Δ h (m)	Δ P (Pa)	
160	-46.5	206.5	0.0249	243.2	36.7 Pa (15.1 %)

Table 3. Comparison between numerical simulation and experimental results for the RPT C1.4C, z = 0 m, y = 0.00071 m, RPT position y = 0 m (lying on invert).

6. Conclusion

Detailed centreline velocity measurements in air and water were undertaken using the roving Preston tube and Prandtl-Pitot tube. The roving Preston tube reference pressure readings varied significantly from the Prandtl-Pitot tube static pressure readings and were affected by proximity to fixed boundaries and varying flow conditions. Numerical modelling showed that the local flow region on the leeward side of the RPT total head tube resulted in a static pressure deficit adjacent to the orifice of the reference pressure tube. This static pressure deficit was difficult to reconcile using simple relationships derived from dimensional analysis. Furthermore, the numerical simulation revealed complex three-dimensional flow adjacent to the reference pressure tube orifice that hindered attempts to apply simple canonical flow analogies. This made the application of Bernoulli's relationship to calculate local time-averaged velocity rather tenuous. Bulk calibration methods were examined to account for the observed static pressure deficit. However, it was acknowledged that these methods were empirical, limited in predictive power, and inaccurate in calculating both wetted perimeter velocities and subsequent quantification of local boundary shear stress. Overall, whilst the flexibility of the RPT was acknowledged, the description of hydrodynamics adjacent to the RPT reference pressure tube, further highlighted the importance of further research in this area, as well as investigating design modifications that can better approximate local static pressures.

References

Bailey, S., Vallilivi, M., Hultmark, M. & Smits, A. 2014, Estimating the value of von Karman's Constant in Turbulent Pipe Flow, *Journal of Fluid Mechanics*, 749, 79-98.

Birkhoff, G. & Zarantonello, E. 1957. *Jets Wakes and Cavities*. Academic Press, New York, 353pp.

Chanson, H. 2020, Low Velocity Zone in Smooth Pipe Culvert with and without Streamwise Rib for Fish Passage, *Journal of Hydraulic Engineering*, 146(9), 10 pp.

Chue, S.H. 1975, Pressure probes for fluid measurement. *Prog in Aero Sc.*, 16(2), 147-223.

Folsom, R. 1956, Review of the Pitot Tube, *Transactions of ASME*, 78, 1447-1460.

Macintosh, J. 1990, Hydraulic Characteristics in Channels of Complex Cross-Section. *Ph.D. thesis*, University of Queensland, Dept of Civil Engineering, Australia, 487 pp.

Macintosh, J., & Isaacs, L. 1992, RPT – The Roving Preston Tube, *Proceedings of the 11th AFMC Australasian Fluid Mechanics Conference*, Hobart, Australia, 2, 1049-1052.

Sanchez, P.X., Leng, X., and Chanson, H. 2018, Fluid Dynamics and Secondary Currents in an Asymmetrical Rectangular Canal with Sidewall Streamwise Rib. *Hydraulic Model Report No. CH113/18*, School of Civil Engineering, University of Queensland, Brisbane, Australia, 158 pp.

Sanchez, P.X., Leng, X., and Chanson, H. 2021, Hydrodynamics and Secondary Currents in an Asymmetrical Rectangular Canal with Streamwise Beam. *J Hydraulic Research*, 59(1), 88-99.